Showcasing research from Dr Matthew Cliffe's laboratory, School of Chemistry, University of Nottingham, UK.

Magnetic order in a metal thiocyanate perovskite-analogue

This study showed that the coordination framework $Cr[Bi(SCN)_6].xH_2O$ undergoes long-range magnetic order, despite the long distance between the two metal sites, a through-bond distance of 15 Å (via eight-bonds). Rietveld refinement of neutron diffraction data measured at the Institut Laue Langevin uncovered that this compound has a Type-II antiferromagnetic order, analogous to that of MnO.

As featured in:

See Matthew J. Cliffe *et al.*, *CrystEngComm*, 2022, **24**, 7250.

rsc.li/crystengcomm

Magnetic order in a metal thiocyanate perovskite-analogue†

Matthew J. Cliffe, ✳[a] Oscar Fabelo[bc] and Laura Cañadillas-Delgado[b]

Metal thiocyanate perovskite-analogues are a growing class of materials, but although they contain paramagnetic cations there have been no reports of their magnetic properties. Due to the large separations between the paramagnetic cations, with a shortest through-bond distance of 15.1 Å, these materials might be expected to be good examples of paramagnets. In this communication we investigate the magnetic properties of a metal thiocyanate framework $Cr[Bi(SCN)_6]\cdot xH_2O$. We find that $Cr[Bi(SCN)_6]\cdot xH_2O$ undergoes long-range magnetic order at $T_N = 4.0(2)$ K. We use neutron powder diffraction to determine that $Cr[Bi(SCN)_6]\cdot xH_2O$ has a MnO-type $\{111\}_{cubic}$-ordering as its ground state, consistent with frustrated nearest- and next-nearest-neighbour antiferromagnetic interactions. This suggests that appropriate design of metal thiocyanate perovskite-analogue structures may reveal a rich vein of frustrated magnetism.

Molecule-based perovskite-analogues, framework compounds built from corner-sharing octahedra with a general formula A_xMX_3 where at least one of A, M or X is a molecular ion, offer a diverse range of new chemistries and functionality to the solid state scientist.[1,2] In particular, including molecular components generates additional degrees of freedom, which permits orderings impossible in conventional atomic analogues—for example, ordering of the electric dipole of $MeNH_3^+$ as an A-site guest can generate electrical polarisation.[3,4] This polar ordering could, if combined with

magnetic order generated by M-site cations, generate multiferroic materials possessing simultaneous electric and magnetic order.[3,5] The magnetism of molecule-based perovskites has therefore been intensively investigated, particularly focussing on metal formates due to the diversity of A-site ammonium and M-site transition metal cations which can be incorporated. A wide range of magnetic formates have now been investigated, with particular excitement found in the wide-range of non-collinear magnets, including the perovskite $A[M(CHOO)_3]$[6–8] and niccolite mixed-metal formates $A\{M[M'(CHOO)_6]\}$.[9–11]

A major challenge for molecular magnetism has been the weakness of the magnetic interactions between paramagnetic ions, especially compared to the pure elements and simple oxides, where strong exchange can be produced through direct overlap of the magnetic orbitals, or a single intervening anion. Developing our understanding of how crystal chemistry determines magnetic interactions will aid us realising both in producing practical magnetism, and, critically, in targeting exotic magnetic phases requiring careful balance of interactions. The cyanide Prussian Blue analogues provide an outstanding example of how crystal engineering can be used to optimise magnetic properties, with the enhancement of magnetic Curie temperatures T_C from 5.6(1) K for Prussian Blue itself, $Fe_4[Fe(CN)_6]_3\cdot xH_2O$,[13] up to 376 K, $KV[Cr(CN)_6]$.[14]

Thiocyanate as a pseudohalide ligand is well-known for its optical properties,[12,15] but control over its magnetism is much less developed, with most focus either on either the two dimensional pseudobinaries[16–19] or frameworks incorporating additional organic coligands.[17,20–22] Recently, some of us showed that the magnetism of the layered pseudobinary $M(NCS)_2$, M = Cu, Ni, Co, Fe and Mn, can be qualitatively explained on the basis of changing orbital occupation and size, leading to enhancement of interactions and uncovering layered antiferromagnetism.[18,19] Three dimensionally connected, perovskite-analogue structured materials would be of particular interest as magnets, but thus

a School of Chemistry, University Park, Nottingham, NG7 2RD, UK.
E-mail: matthew.cliffe@nottingham.ac.uk
b Institut Laue-Langevin, 6 rue Jules Horowitz, BP 156, 38042 Grenoble Cedex 9, France
c Departamento de Física, Universidad de La Laguna, Avda. Astrofísico Fco. Sánchez s/n, 38204 La Laguna, Tenerife, Spain

far no frameworks containing only paramagnetic metals on the M-site has been synthesised, as the sulfur terminus requires a softer metal such as Cd^{2+},[23] Bi^{3+},[12] or Pt^{4+},[24] leading to the "double perovskite" structure. These sulfur-bonding metals are all diamagnetic, which suggests that the paramagnetic ions in thiocyanate Prussian Blue analogues would be magnetically isolated. However, were these paramagnetic metal ions to be magnetically connected through superexchange pathways, these frameworks would be examples of magnets with the $J_1 - J_2$ face-centered cubic model [Fig. 1(b)], which is both the source of exotic frustrated states,[25,26] and shared by both rock-salt structured oxides[27,28] and double perovskites.[29–31]

Here, we report the magnetic properties of a metal double-perovskite framework, $Cr[Bi(SCN)_6]\cdot xH_2O$ [Fig. 1], using a combination of bulk magnetometry and neutron powder diffraction. We show that despite the large distances (>8 Å) between paramagnetic ions, there is significant superexchange coupling between these ions: indeed, we find that it has long-range magnetic order below 4.0(2) K. We then go on to solve the magnetic structure of $Cr[Bi(SCN)_6]\cdot xH_2O$, demonstrating that it orders with ferromagnetically correlated close-packed $\{111\}_{cubic}$ type planes, antiferromagnetically coupled, like MnO.[27,32] This finding suggests that by using the extensive range of chemistry available in perovskite-analogue metal thiocyanates we could tune the magnetic interactions to realise exotic quantum states.

A multigram sample of $Cr[Bi(SCN)_6]\cdot xH_2O$ was prepared *via* solution precipitation, in which an aqueous solution of $K_3Cr(NCS)_6\cdot 4H_2O$ (5.89 g, 10 mmol) was added to a solution of $Bi(NO_3)_3\cdot 5H_2O$ (4.85 g, 10 mmol) in 2 M HNO_3, stirred for 2 hours, filtered, washed with water and dried.[12] We confirmed the structure of this compound using powder diffraction, and from the lattice parameters we determined that this sample was hydrated ($x \approx 1$) [ESI† Fig. S3].[12] We me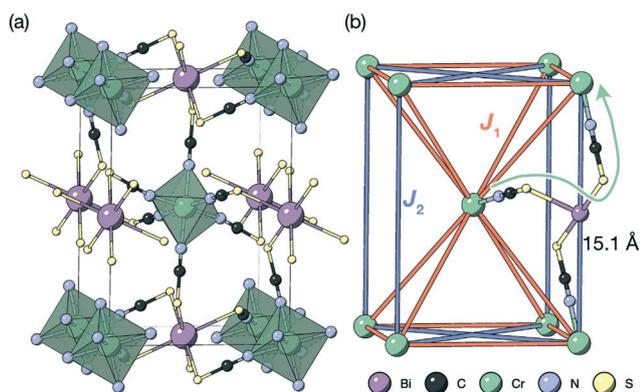asured the magnetisation in a 100 Oe applied field using an MPMS-3 magnetometer on warming from a sample cooled in zero field, calculating the susceptibility using the small field approximation.

The susceptibility showed a sharp cusp at 4.0 K and Curie Weiss fitting to the high temperature susceptibility (20–300 K, including a temperature independent paramagnetism term) gave a Weiss temperature, θ, of −7.8(2) K, and an effective moment of 3.27(0.06) μ_B, reduced from the spin-only value of 3.87 μ_B [Fig. 2]. Isothermal magnetisation measurements at 2 K and 5 K showed no evidence of hysteresis, with a field-induced transition at around 1.4(1) T observed in the data measured at 2 K [ESI† Fig. S4 and S5]. Together, this suggests that $Cr[Bi(SCN)_6]\cdot H_2O$ is an antiferromagnet, with mildly frustrated ratio of $f = |\theta|/T_N = 1.9$.

To confirm that the ground state was indeed long-range magnetic antiferromagnetic order, we carried constant wavelength powder neutron diffraction measurements on the high-intensity medium resolution D1B diffractometer at ILL, Grenoble [Fig. 3, ESI† S1 and S2].[33] The incident wavelength was λ = 2.52 Å and the scattering was measured over an angular range of $2 < 2\theta < 128°$. We measured high quality long-acquisition time diffraction patterns at 10 K and 2 K, supplemented by shorter measurements at intermediate temperatures of 5, 4.5, 4, 3.5, 3 and 2.5 K. By subtracting the 10 K dataset from the lower temperature data we were able to confirm that additional magnetic Bragg peaks emerged between 4 and 4.5 K [Fig. 3], demonstrating that the cusp identified in bulk magnetic susceptibility was due to antiferromagnetic order. We first refined the structural model against the previously determined room temperature
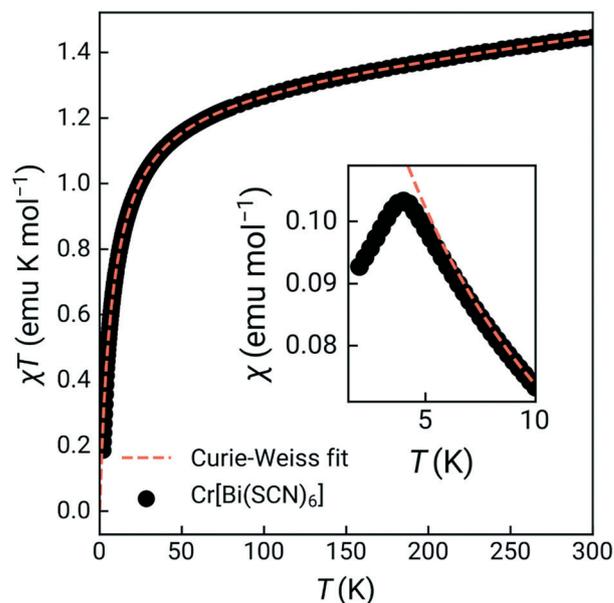

Fig. 1 (a) Crystal structure of the $Cr[Bi(SCN)_6]$ framework. Disordered guest water omitted for clarity.[12] (b) The structure showing only the magnetic Cr^{3+} ions and the nearest- (J_1) and next-nearest-neighbour (J_2) superexchange pathways, together with the through-bond distance.

Fig. 2 Variable temperature magnetic susceptibility product measured over the range 2–300 K (zero field cooled). Inset shows the magnetic susceptibility measured over 2–10 K, highlighting magnetic order. Orange dashes line indicates the Curie–Weiss fit, carried out over the range 20 to 300 K.
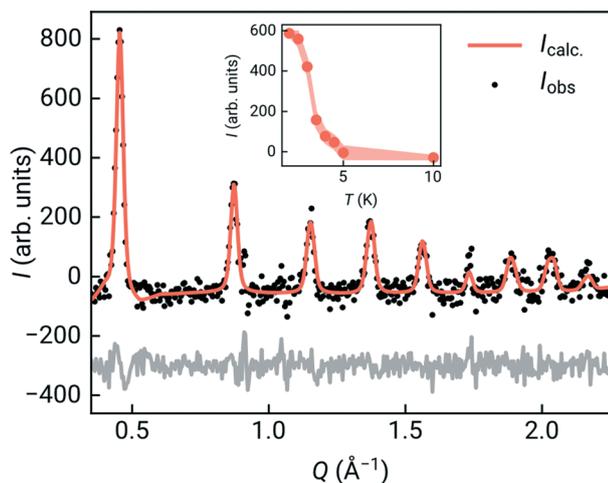
Fig. 3 Detail of the magnetic Rietveld refinement on the P_c2_1/n Shubnikov space group, showing all observed magnetic Bragg peaks. The magnetic contribution has been isolated by subtracting the paramagnetic contribution (10 K). Observed (black points) and calculated (orange solid line) powder diffraction pattern (magnetic R_{Bragg} = 7.77). The observed-calculated difference pattern is depicted as a grey line at the bottom of the figure. Inset depicts the temperature dependence of the intensity of the first observed magnetic Bragg line obtained through Gaussian fitting of a single line.

structure in space group $P2_1/n$ of $Cr[Bi(SCN)_6]\cdot xH_2O$ to determine the overall scale and unit cell parameters using the Rietveld method and the FullProf software suite, giving a = 8.3312(16) Å, b = 8.3805(17) Å, c = 11.9723(15) Å, β = 90.30(3)° [ESI† Fig. S2].[34]

We began our determination of the magnetic structure by indexing the additional magnetic reflections with reference to the pseudocubic $Fm\bar{3}m$ $\sqrt{2} \times \sqrt{2} \times 1$ supercell, because the magnetic lattice has near-cubic metrical symmetry: $\sin\beta = 5 \times 10^{-6}$, $a/V^{\frac{1}{3}} = a/a_{cubic} = -0.74\%$, $b/a_{cubic} = -0.09\%$, $c/a_{cubic} = +0.84\%$. This gave us a propagation vector of $k_{cubic} = \left(\frac{1}{2}\frac{1}{2}\frac{1}{2}\right)$.

This will correspond, for a simple collinear antiferromagnet, to ferromagnetically correlated close packed $\{111\}_{cubic}$ planes coupled antiferromagnetically. However, accounting for the true monoclinic $P2_1/n$ symmetry of the nuclear structure splits this pseudocubic propagation vector into two inequivalent propagation vectors: $\left(0\frac{1}{2}\frac{1}{2}\right)$ and $\left(\frac{1}{2}0\frac{1}{2}\right)$, the E and Y points on the Brillouin zone boundary, respectively. This reflects the fact the $\{111\}_{cubic}$-type close-packed planes are symmetry- and chemically-distinct in this material. Using the k-search program included in the FullProf suite[34] to quantitatively assess the propagation vectors revealed both the $\left(0\frac{1}{2}\frac{1}{2}\right)$ and $\left(\frac{1}{2}0\frac{1}{2}\right)$ vectors, with a slightly better fit for $\left(\frac{1}{2}0\frac{1}{2}\right)$, Y, than $\left(0\frac{1}{2}\frac{1}{2}\right)$, E, (figure of merit = 0.37 *vs.* 0.82).

Using the ISODISTORT tool from the ISOTROPY software suite,[35] we were able to identify the three distinct possible

irreducible representations (irreps) consistent with this family of propagation vectors that produce a non-zero magnetic moment: $mE_1 + E_2$, mY_1 and mY_2 (Miller and Love notation).[36] These three models correspond to the magnetic spaces groups $P_S\bar{1}$ ($mE_1 + E_2$) and P_c2_1/n (mY_1, mY_2). We were able to achieve a good Rietveld refinement fit to models for all three of these structures, in each case leading to structure consisting approximately of ferromagnetically correlated $\{111\}_{cubic}$ layers antiferromagnetically coupled. These structures are nearly collinear with moments lying nearly within the $\{111\}_{cubic}$ plane with small tilts of the moments away from the primary axis (*ca.* 6°), though the high degree of pseudosymmetry meant our determination of the relative angles of the moment is not completely unambiguous. We were able to refine the magnitude of the Cr^{3+} giving M = 2.45(20) μ_B, which is approximately 80% of the anticipated spin-only value. This small deviation is likely explained by the combination of some covalency and comparatively high scaled measurement temperature (T/T_N = 0.5). The main difference between the models was which of the four $\{111\}_{cubic}$ type planes the spins ordered ferromagnetically within: the mY models ordered in the $(1\bar{1}1)_{cubic}$ or $(10\bar{1})$ planes and the $mE_1 + E_2$ model ordered in the $(11\bar{1})_{cubic}$ or $(01\bar{1})$ planes. We found that the mY_1 model fitted the data best and as the $mE_1 + E_2$ is in addition a lower symmetry triclinic structure with two symmetry independent moments, we therefore think the mY_1 model is likely to be correct structure [Fig. 4]. Single crystal neutron diffraction data would allow for completely unambiguous determination of
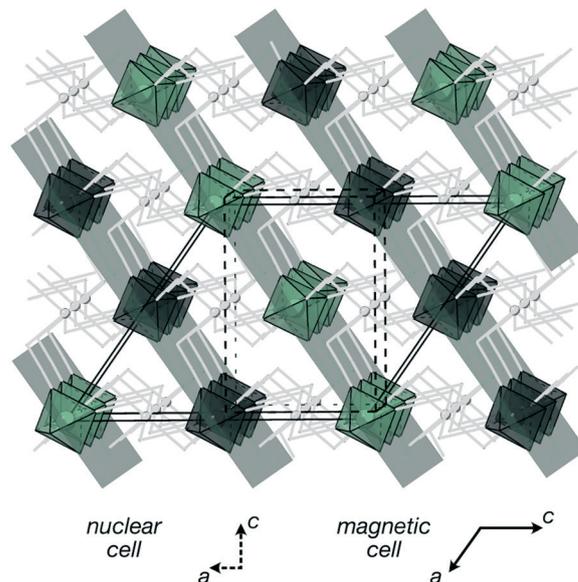

Fig. 4 Magnetic structure of $Cr[Bi(SCN)_6]\cdot xH_2O$. Magnetic Cr atoms are coloured in green and black to illustrate their relative orientations, and the other non-magnetic framework atoms are shown in grey. The $\{111\}_{cubic}$ type planes in which all spins are ferromagnetically correlated are highlighted. The magnetic and nuclear unit cells are related as follows: $a_{mag} = a_{nuc} - c_{nuc}$, $b_{mag} = -b_{nuc}$ and $c_{mag} = -2a_{nuc}$.

the magnetic structure but as yet single crystals of sufficient size are unavailable.

The most striking feature of this order is that it occurs at such accessible temperatures. The shortest through space distance between Cr atoms is $d = 8.32$ Å, and the shortest through-bond distance is $d = 15.1$ Å, and occurs through 8-bond superexchange, Cr–N–C–S–Bi–S–C–N–Cr. This can be compared to the iron cyanide Prussian Blue, which orders ferromagnetically at 5.6(1) K[13] with the magnetic Fe^{3+} ions separated by 7.2 Å, where magnetic superexchange occurs through a six-bond Fe^{3+}–N–C–Fe^{2+}–C–N–Fe^{3+} pathway 10.2 Å long. In Prussian Blue, charge and spin delocalisation onto Fe^{2+} (approximately 5% of an electron) through a mixed-valence mechanism are critical to the generation of long-range order.[37,38] Mixed valency is not likely in this case as the adjacent oxidation states for both Cr and Bi are not easily accessible, and the antiferromagnetic interactions we observe rule out the ferromagnetic 'double exchange' found in Prussian Blue. On possible explanation would be facilitation of this comparatively strong superexchange through the accessible NCS redox states—as can be see in the relatively dispersive conduction band in our previously reported DFT band-structure calculations of Cr[Bi(SCN)$_6$].[12]

The importance of effective superexchange can be seen by comparison to paramagnetic salts of Cr^{3+}, _e.g._ [Cr(CN)$_6$][Co(NH$_3$)$_6$], where $|\theta| < 0.05$ K and $d_{Cr-Cr} = 7.4$ Å.[39] These comparisons also allow us to eliminate through-space dipolar coupling as a significant contributor to the observed order. Indeed, even in molecular cluster nanomagnets with similar magnet–magnet spacing but much larger total spin it is clear that superexchange rather than dipolar order drives the transition to magnetic long-range order, _e.g._ the $S = 35/2$ [Fe$_{19}$ (metheidi)$_{10}$(OH)$_{14}$O$_6$(H$_2$O)$_{12}$]NO$_3 \cdot 24$H$_2$O has a shortest Fe–Fe distance of 8.3 Å and orders at 1.2 K due to superexchange interactions.[40]

The Cr ions form a face-centered cubic lattice, with only small chemical differences between different crystallographic directions. The interactions are likely to be primarily through-bond rather than through space, and as such the nearest neighbour (J_1) and next nearest neighbour (J_2) interactions are likely to be comparable in magnitude [Fig. 1(b)]. This is directly analogous to what has been found in both rocksalt transition metal monoxides, _e.g._ the canonical MnO,[27,32] and the oxide double perovskites.[29] The {111}$_{cubic}$ AFM order observed (Type II) occurs for $J_2 > 0.5J_1$ for an ideal $J_1 - J_2$ face-centred cubic magnet with antiferromagnetic interactions. The combination of this with the observed mild frustration, $|\theta|/T_N = 1.9$, and the presumed weakness of both further-neighbour superexchange (due to the long distances) and of non-Heisenberg effects due to the Cr^{3+} ion presence suggests that suggests that $J_2 < J_1$, and thus that a small (20%) reduction in J_1/J_2 might induce a transition into a highly frustrated state.[41,42] Like other perovskites, Cr[Bi(SCN)$_6$] has a wide-range of potential chemical possibilities for tuning its magnetic function: not only through substitution of the magnetic Cr,[12] but also of

the non-magnetic Bi,[23,24] and the anionic ligand[43] or the inclusion of A-site cations.[44] This, together with the moderate exchange strength found in this material, comparable with the Zeeman splitting accessible through superconducting magnets, suggests that NCS double pervoskites are ideal platforms to engineer the complex, chiral, multi-k magnetic orderings of current interest for their potential use in magnetic computation.[26,45]

Author contributions

M. J. C. synthesized the samples. M. J. C., O. F., and L. C. D. carried out the neutron diffraction experiment and analysed the neutron diffraction data. M. J. C. carried out and analysed the bulk magnetic measurements. M. J. C. wrote the paper, with input from all other authors.

Conflicts of interest

There are no conflicts to declare.

Acknowledgements

Notes and references

1 W. Li, Z. Wang, F. Deschler, S. Gao, R. H. Friend and A. K. Cheetham, _Nat. Rev. Mater._, 2017, **2**, 16099.

2 H. A. Evans, Y. Wu, R. Seshadri and A. K. Cheetham, _Nat. Rev. Mater._, 2020, **5**, 196–213.

3 D.-W. Fu, W. Zhang, H.-L. Cai, Y. Zhang, J.-Z. Ge, R.-G. Xiong, S. D. Huang and T. Nakamura, _Angew. Chem., Int. Ed._, 2011, **50**, 11947–11951.

4 H. L. B. Boström, M. S. Senn and A. L. Goodwin, _Nat. Commun._, 2018, **9**, 2380.

5 M. S. Senn and N. C. Bristowe, _Acta Crystallogr., Sect. A: Found. Adv._, 2018, **74**, 308–321.

6 X.-Y. Wang, L. Gan, S.-W. Zhang and S. Gao, _Inorg. Chem._, 2004, **43**, 4615–4625.

7 Z. Wang, B. Zhang, T. Otsuka, K. Inoue, H. Kobayashi and M. Kurmoo, _Dalton Trans._, 2004, 2209–2216.

8 L. Cañadillas-Delgado, L. Mazzuca, O. Fabelo, J. Rodríguez-Carvajal and V. Petricek, _Inorg. Chem._, 2020, **59**, 17896–17905.

9 L. Mazzuca, L. Cañadillas-Delgado, J. A. Rodríguez-Velamazán, O. Fabelo, M. Scarrozza, A. Stroppa, S. Picozzi, J.-P. Zhao, X.-H. Bu and J. Rodríguez-Carvajal, _Inorg. Chem._, 2017, **56**, 197–207.

10 K. S. Hagen, S. G. Naik, B. H. Huynh, A. Masello and G. Christou, *J. Am. Chem. Soc.*, 2009, **131**, 7516–7517.

11 L. Cañadillas-Delgado, O. Fabelo, J. A. Rodríguez-Velamazán, M. H. Lemée-Cailleau, S. A. Mason, E. Pardo, F. Lloret, J. P. Zhao, X. H. Bu, V. Simonet, C. V. Colin and J. Rodríguez-Carvajal, *J. Am. Chem. Soc.*, 2012, **134**, 19772–19781.

12 M. J. Cliffe, E. N. Keyzer, M. T. Dunstan, S. Ahmad, M. F. L. De Volder, F. Deschler, A. J. Morris and C. P. Grey, *Chem. Sci.*, 2019, **10**, 793–801.

13 F. Herren, P. Fischer, A. Ludi and W. Haelg, *Inorg. Chem.*, 1980, **19**, 956–959.

14 M. Verdaguer and G. S. Girolami, in *Magnetism: Molecules to Materials V*, ed. J. S. Miller and M. Drillon, WILEY-VCH Verlag, Weinheim, 2005, vol. 36, pp. 283–346.

15 J. J. Berzelius, *Lehrbuch der Chemie*, 1826, vol. 2, p. 771.

16 G. C. DeFotis, K. D. Dell, D. J. Krovich and W. W. Brubaker, *J. Appl. Phys.*, 1993, **73**, 5386–5388.

17 E. Shurdha, S. H. Lapidus, P. W. Stephens, C. E. Moore, A. L. Rheingold and J. S. Miller, *Inorg. Chem.*, 2012, **51**, 9655–9665.

18 M. J. Cliffe, J. Lee, J. A. M. Paddison, S. Schott, P. Mukherjee, M. W. Gaultois, P. Manuel, H. Sirringhaus, S. E. Dutton and C. P. Grey, *Phys. Rev. B*, 2018, **97**, 144421.

19 E. N. Bassey, J. A. M. Paddison, E. N. Keyzer, J. Lee, P. Manuel, I. da Silva, S. E. Dutton, C. P. Grey and M. J. Cliffe, *Inorg. Chem.*, 2020, **59**, 11627–116339.

20 J. Werner, Z. Tomkowicz, T. Reinert and C. Näther, *Eur. J. Inorg. Chem.*, 2015, **2015**, 3066–3075.

21 S. Baran, A. Hoser, M. Rams, S. Ostrovsky, T. Neumann, C. Näther and Z. Tomkowicz, *J. Phys. Chem. Solids*, 2019, **130**, 290–297.

22 E. Shurdha, C. E. Moore, A. L. Rheingold, S. H. Lapidus, P. W. Stephens, A. M. Arif and J. S. Miller, *Inorg. Chem.*, 2013, **52**, 10583–10594.

23 K.-P. Xie, W.-J. Xu, C.-T. He, B. Huang, Z.-Y. Du, Y.-J. Su, W.-X. Zhang and X.-M. Chen, *CrystEngComm*, 2016, **18**, 4495–4498.

24 H. Tabe, M. Matsushima, R. Tanaka and Y. Yamada, *Dalton Trans.*, 2019, **48**, 17063–17069.

25 M. V. Gvozdikova and M. E. Zhitomirsky, *JETP Lett.*, 2005, **81**, 236–240.

26 P. Balla, Y. Iqbal and K. Penc, *Phys. Rev. Res.*, 2020, **2**, 043278.

27 A. L. Goodwin, M. G. Tucker, M. T. Dove and D. A. Keen, *Phys. Rev. Lett.*, 2006, **96**, 047209.

28 L. Timm, M. G. Tucker, D. A. Keen, P. M. M. Thygesen, P. J. Saines and A. L. Goodwin, *Phys. Scr.*, 2016, **91**, 114004.

29 C. R. Wiebe, J. E. Greedan, P. P. Kyriakou, G. M. Luke, J. S. Gardner, A. Fukaya, I. M. Gat-Malureanu, P. L. Russo, A. T. Savici and Y. J. Uemura, *Phys. Rev. B*, 2003, **68**, 134410.

30 O. H. J. Mustonen, C. E. Pughe, H. C. Walker, H. M. Mutch, G. B. G. Stenning, F. C. Coomer and E. J. Cussen, *Chem. Mater.*, 2020, **32**, 7070–7079.

31 S. Kanungo, B. Yan, C. Felser and M. Jansen, *Phys. Rev. B*, 2016, **93**, 161116.

32 C. G. Shull and J. S. Smart, *Phys. Rev.*, 1949, **76**, 1256–1257.

33 I. P. Orench, J. F. Clergeau, S. Martínez, M. Olmos, O. Fabelo and J. Campo, *J. Phys.: Conf. Ser.*, 2014, **549**, 012003.

34 J. Rodríguez-Carvajal, *Phys. B*, 1993, **192**, 55–69.

35 H. T. Stokes, D. M. Hatch and B. J. Campbell, ISOTROPY Software Suite.

36 A. P. Cracknell, B. L. Davies, S. C. Miller and W. F. Love, *Kronecker Product Tables*, Plenum, New York, 1979, vol. 1.

37 B. Mayoh and P. Day, *J. Chem. Soc., Dalton Trans.*, 1976, 1483–1486.

38 P. Day, F. Herren, A. Ludi, H. U. Güdel, F. Hulliger and D. Givord, *Helv. Chim. Acta*, 2007, **63**, 148–153.

39 R. L. Carlin, R. Burriel, J. Pons and J. Casabo, *Inorg. Chem.*, 1983, **22**, 2832–2836.

40 F. L. Pratt, T. Guidi, P. Manuel, C. E. Anson, J. Tang, S. J. Blundell and A. K. Powell, *Magnetochemistry*, 2021, **7**, 74.

41 Y. Yamamoto and T. Nagamiya, *J. Phys. Soc. Jpn.*, 1972, **32**, 1248–1261.

42 N.-N. Sun and H.-Y. Wang, *J. Magn. Magn. Mater.*, 2018, **454**, 176–184.

43 T. Neumann, M. Rams, Z. Tomkowicz, I. Jess and C. Näther, *Chem. Commun.*, 2019, **55**, 2652–2655.

44 J. Y. Lee, S. Ling, S. P. Argent, M. S. Senn, L. Cañadillas-Delgado and M. J. Cliffe, *Chem. Sci.*, 2021, **12**, 3516–3525.

45 S. Mühlbauer, B. Binz, F. Jonietz, C. Pfleiderer, A. Rosch, A. Neubauer, R. Georgii and P. Böni, *Science*, 2009, **323**, 915–919.